Efficient conversion of NO to NO2 on SO2-aged MgO under atmospheric conditions

Journal:	*Environmental Science & Technology*
Manuscript ID	es-2020-05071k.R1
Manuscript Type:	Article
Date Submitted by the Author:	04-Sep-2020
Complete List of Authors:	Liu, Chang; Chinese Academy of Meteorological Sciences, Wang, Honghong; Research Centre for Eco-Environmental Sciences Chinese Academy of Sciences, State Key Joint Laboratory of Environment Simulation and Pollution Control Ma, Qingxin; Chinese Academy of Sciences, Research Center for Eco-Environmental Sciences Ma, Jinzhu; Chinese Academy of Sciences, Research Center for Eco-Environmental Sciences Wang, Zhe; Hong Kong University of Science and Technology, Division of Environment and Sustainability Liang, Linlin; Institute of Atmospheric Composition Chinese Academy of Meteorological Sciences, Xu, Wanyun; Chinsese Academy of Meterological Sciences, Institute of Atmospheric Composition Zhang, Gen; State Key Laboratory of Severe Weather & Key Laboratory of Atmospheric Chemistry of CMA, Chinese Academy of Meteorological Sciences Zhang, Xiaoye; State Key Laboratory of Severe Weather & Key Laboratory of Atmospheric Chemistry of China Meteorological Administration Wang, Tao; Hong Kong Polytechnic University, Civil & Structural Engineering He, Hong; Chinese Academy of Sciences, Research Center for Eco-Environmental Sciences

Efficient conversion of NO to NO_2 on SO_2-aged MgO under atmospheric conditions

Chang Liu[a,b,§], Honghong Wang[c,d,§], Qingxin Ma[b,c,d,e], Jinzhu Ma[c,d,e], Zhe Wang[f], Linlin Liang[a], Wanyun Xu[a], Gen Zhang[a], Xiaoye Zhang[a,d], Tao Wang[b], Hong He[c,d,e]*

[a] State Key Laboratory of Severe Weather & Key Laboratory of Atmospheric Chemistry of China Meteorological Administration, Chinese Academy of Meteorological Sciences, Beijing 100081, China

[b] Department of Civil and Environmental Engineering, the Hong Kong Polytechnic University, Kowloon, Hong Kong 999077, China

[c] State Key Joint Laboratory of Environment Simulation and Pollution Control, Research Center for Eco-Environmental Sciences, Chinese Academy of Sciences, Beijing 100085, China

[d] Center for Excellence in Urban Atmospheric Environment, Institute of Urban Environment, Chinese Academy of Sciences, Xiamen 361021, China

[e] College of Resources and Environment, University of Chinese Academy of Sciences, Beijing 100049, China

[f] Division of Environment and Sustainability, The Hong Kong University of Science and Technology, Kowloon, Hong Kong

ABSTRACT

NO-NO_2 cycle determines the formation of O_3 and hence plays a critical role in the oxidizing capacity of troposphere. Traditional view concluded that the heterogeneous oxidation of NO to NO_2 was negligible due to the weak reactivity of NO on aerosols compared to homogeneous oxidation process. However, the results here reported the first time that SO_2 can greatly promote the heterogeneous transformation of NO to NO_2 and HONO on MgO particles under ambient condition. The uptake coefficients of NO were increased by 2-3 orders of magnitudes on SO_2-aged MgO compared to fresh sample. Based on spectroscopic characterization and density functional theory (DFT) calculations, the active sites for the adsorption and oxidation of NO were determined to be sulfates, where an intermediate [SO_4-NO] complex was formed during the adsorption. The decomposition of this species led to the formation of NO_2 and the change of sulfate configuration. The formed NO_2 could further react with surface sulfite to form HONO and sulfate. The conversion of NO to NO_2 and HONO on SO_2-aged MgO surface under ambient condition contributes a new formation pathway of NO_2 and HONO, and could be quite helpful for understanding the source of atmospheric oxidizing capacity as well as the formation of air pollution complex in polluted regions such as the northern China.

36 **TOC ART**

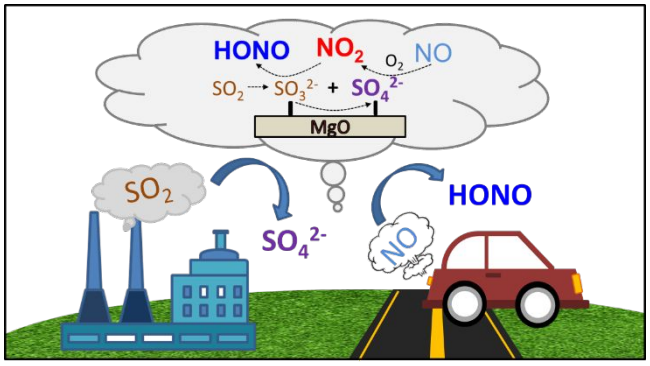

37

38

INTRODUCTION

The importance of nitrogen oxides (NOx = NO + NO_2) in atmospheric chemistry is their role in the determination of O_3 formation.[1] NOx are introduced into the troposphere primarily in the form of NO.[2] For example, NO contributes approximately 90% NOx in vehicles with selective catalytic reduction (SCR) system.[3-6] NO is further oxidized to NO_2 by oxidants in the atmosphere. The photolysis of NO_2 results in the formation of NO and ground-state oxygen, $O(^3P)$ atoms, which further reacts with O_2 to produce O_3 in the troposphere. Thus, the oxidation of NO to NO_2 is of particular importance in the formation of O_3 and hence determines the oxidizing capacity of troposphere. The homogeneous oxidation of NO to NO_2 by O_2 has been widely studied and the reaction rate was proved to be quite slow under room temperature.[7, 8] Gaseous oxidants including ozone (O_3),[7-9] organic peroxy radicals (RO_2),[10, 11] and hydroperoxy radical (HO_2)[7, 12-14] are efficient to oxidize NO to NO_2.

The oxidation of NO to NO_2 is also a key step both in the NOx reduction technologies as well as the nitric acid production.[15-17] For example, the NH_3-SCR reaction rate can be greatly enhanced if a fraction of NO is converted to NO_2, and the increase of NO_2 content greatly improves the efficiency of the reduction catalysts and also decreases aging of the catalysts.[16, 18] Supported catalysts (included noble metals and metal oxides) are widely used in the catalytic oxidation of NO.[19-21] However, these oxidation reactions always conducted under high NO concentration (up to hundreds ppm) and high temperature (about 423-723 K).[22-26] In contrast, it was found that when NO concentration was low to ppb level, the heterogeneous reaction of NO on atmospheric particles was slow and supposed to hardly happen.[27, 28] Therefore, the heterogeneous conversion of NO to NO_2 in the atmospheric chemistry has always been neglected.

Recently, synergistic effect between NOx and SO_2 have been found in field campaigns, laboratory experiments and model simulations.[29-34] Both coexisting NO_2[35-39] and NO[40] were found to improve the conversion of SO_2 to sulfate on mineral dust due to the oxidizability of NO_2. On the other hand, SO_2 was also demonstrated to change the reaction pathways of NO_2 in these heterogeneous reactions on mineral dust. For example, N_2O_4 was detected as an intermediate on the surface of mineral oxides while 100 ppm NO_2 and 100 ppm SO_2 were coexisting.[35] Our previous research found that when the concentration of NO_2 and SO_2 was decreased to 100 ppb, SO_2 can initiate the efficient conversion of NO_2 to nitrous acid (HONO) on MgO surface.[41] It should be noted that the production of NO was not observed during this redox reaction between NO_2 and SO_2. However, previous studies observed NO as a product in the heterogeneous uptake of NO_2 on mineral oxides.[42, 43] It implies that the coexisting SO_2 not only plays an important role in the heterogeneous uptake of NO_2, but also may affect the interface process of NO. However, the latter is poorly understood.

In this study, we further explored the role of coexisting SO_2 as well as the sulfate species on the heterogeneous reaction of NO on MgO. MgO is considered to be a typical constituent of dust aerosols, and is widely used as a model oxide for the study of trace gas heterogeneous reactions.[41, 44-47] Coated-wall flow tube reactor, *in situ* diffuse reflectance Fourier transformed infrared spectroscopy (*in situ* DRIFTS), and density functional theory (DFT) calculations were combined to reveal the detailed mechanism and kinetic. A new heterogeneous oxidation mechanism of NO to NO_2 under ambient atmospheric conditions was proposed. To our knowledge, this is the first time to report efficient heterogeneous conversion of NO to NO_2 and HONO on atmospheric particles under atmospheric conditions. This result could give new insight into the atmospheric

nitrogen chemistry, and could help to understand the source of atmospheric oxidizing capacity in polluted regions such as the northern China.

EXPERIMENTAL

Coated-wall flow tube reactor.

The uptake experiments were carried out in a horizontal cylindrical coated-wall flow tube reactor which was previously described.[41] The flow tube reactor was maintained at 295 K by circulating water bath through the outer jacket of the flow tube reactor. The total flow rate of carrier gas (high purity synthetic air) was 0.9 $L \cdot min^{-1}$ to ensure a laminar regime. The relative humidity (RH) for synthetic air was around 5% recorded by a hygrometer (RH-USB, Omega, USA) during the whole experiment. 100 ppb NO was introduced into the flow tube through a movable injector with 0.3 cm radius. The concentrations of NO_2 and NO were online measured using NOx analyzer (42*i*, Thermo Scientific, USA). A long path absorption photometer (LOPAP-O3, QUMA, German) was used to online monitor the concentration of HONO. All experiments were conducted at ambient temperature (295 K) and 5% RH, with the total flow rate 0.9 $L \cdot min^{-1}$.

Preparation of MgO for flow tube experiments.

The suspension of MgO powder (AR, Sigma-Aldrich) dissolved in ultrapure water was dripped uniformly into a quartz tube (20 cm length, 1.1 cm i.d.) and dried overnight in an oven at 373 K. The BET (Brunauer-Emmett-Teller) surface area (S_{BET}) of MgO was measured to be 135.6 $cm^2 \cdot mg^{-1}$. SO_2-aged MgO samples were online prepared during flow tube experiments by exposing

the quartz tube with fresh MgO film to 1 ppm SO_2 in air flow for 4 h, then purged with air for 2 h to remove physically adsorbed surface species.

Uptake coefficient.

The kinetic behavior of NO can be well described by assuming a pseudo first-order reaction with respect to the gas-phase NO concentration. The first-order rate constant (k_{obs}) is related to the geometric uptake coefficient (γ_{geo}) according to the following equation:[42, 48]

$$\frac{d}{dt}ln\frac{C_0}{C_i} = k_{obs} = \frac{\gamma_{geo}\langle c_{NO}\rangle}{2r_{tube}} \quad (1)$$

where r_{tube}, t and $\langle c_{NO}\rangle$ are the flow tube radius (0.3 cm), the exposure time, and the NO average molecular velocity (498 $m \cdot s^{-1}$), respectively. C_0 is the initial NO concentration when there is no contact between the MgO and NO. C_i is the NO concentration detected during the uptake.

If the loss of NO at the particle surface is too rapid to be recovered with the NO supply, a radial concentration gradient in the gas phase will be formed, which may cause diffusion limitations. Therefore, a correction for diffusion in the gas phase should be taken into account. Here, the Cooney-Kim-Davis (CKD) method was used to correct uptake coefficients.[49, 50]

***In situ* diffuse reflectance infrared Fourier transform spectroscopy (*in situ* DRIFTS) measurements.**

The heterogeneous reactions of NO and SO_2 on MgO were also studied by *in situ* DRIFTS (*is*50, Thermo Scientific, USA), equipped with an *in situ* diffuse reflection chamber and a high-sensitivity mercury cadmium telluride (MCT) detector cooled by liquid N_2. Before the experiment, MgO powder was finely ground and placed into a ceramic crucible in the *in situ* chamber. The sample was first pretreated at 373 K for 180 min in air stream with a total flow of 200 $mL \cdot min^{-1}$.

Then after 60 min the temperature was cooled to room temperature (295 K) and the sample was exposed to NO and/or SO_2. The infrared spectra were collected using a computer with OMNIC 6.0 software (Nicolet Corporation, USA). All spectra were recorded at a resolution of 4 cm^{-1} for 100 scans in the spectral range of 600 to 4000 cm^{-1}, and then Kubelka-Munk (K-M) conversion was conducted. The low frequency cutoff of spectra was due to the strong lattice oxide absorption of the samples.

Density functional theory (DFT) calculations.

Geometry optimizations and energy calculations were carried out using the Vienna Ab-initio Simulation Package (VASP 5.4.1).[51] The projected augmented-wave (PAW) method was employed to describe the interactions between ions and electrons.[52, 53] The wave functions and exchange-correlation function were elucidated by plane wave basis set and PBE generalized gradient approximation, respectively.[54] The cutoff energy for the plane-waves was set to 400 eV. The Brillouin zone was sampled using 2 × 3 × 1 k points Monkhorst-Pack grid during the surface and adsorption geometry optimization. The Gaussian smearing method with a smearing width of 0.2 eV was employed to accelerate the convergence of integration at the Brillouin zone. A 4×3 supercell with five atomic layers slab was built for MgO (001) surface. In the computation, the bottom two layers of the slab were fixed and the top three layers and adsorbates were fully relaxed until the forces on each atom were less than 0.02 $eV \cdot Å^{-1}$. A vacuum layer of 15 Å was used to avoid the interactions between the surface slabs. The reaction pathways and transition states were calculated via the climbing image nudged elastic band (CI-NEB) method with a 0.05 $eV \cdot Å^{-1}$ force converged threshold.

The adsorption energies (E_{ads}) of the isolated molecules (*e.g.* NO and NO_2) on the surface were calculated as:

$E_{ads} = E_{slab\text{-}x}\text{-}(E_{slab} + E_x)$ (2)

where E_{slab}, E_x and $E_{slab\text{-}x}$ refers to the energy of the MgO(001) surface slab model, NO or NO_2 in the gaseous phase, and the slab-NO/slab-NO_2 supersystem. According to the above equation, negative values of E_{ads} indicate an exothermic reaction and positive values indicate that adsorption does not occur.

RESULTS AND DISCUSSIONS

NO_2 and HONO formation in NO uptake.

The uptake of NO on fresh and SO_2-aged MgO samples was measured by flow tube experiments. SO_2-aged MgO samples were online prepared by exposing the tube which is covered with fresh MgO to 1000 ppb SO_2 in air flow for 4 h, then purged with air for 2 h to remove physically adsorbed surface species. The change of concentrations of NO, NO_2, and HONO during the uptake were shown in Figure 1. Fresh MgO surface was inactive to NO since no obvious uptake of NO was observed (Figure 1A). Coexisting SO_2 could promote the adsorption of NO and lead to the release of NO_2 and HONO (Figure 1B and Figure 1C), especially when the SO_2 concentration increased to 1000 ppb. When SO_2-aged MgO was exposed to NO, abrupt decrease in the NO concentration and the generation of NO_2 and HONO were also observed (Figure 1D). The blank tests shown in Figure S1 implied that the formation of NO_2 and HONO is not due to the reaction of NO on tube surface or by the gaseous reaction between NO and SO_2.

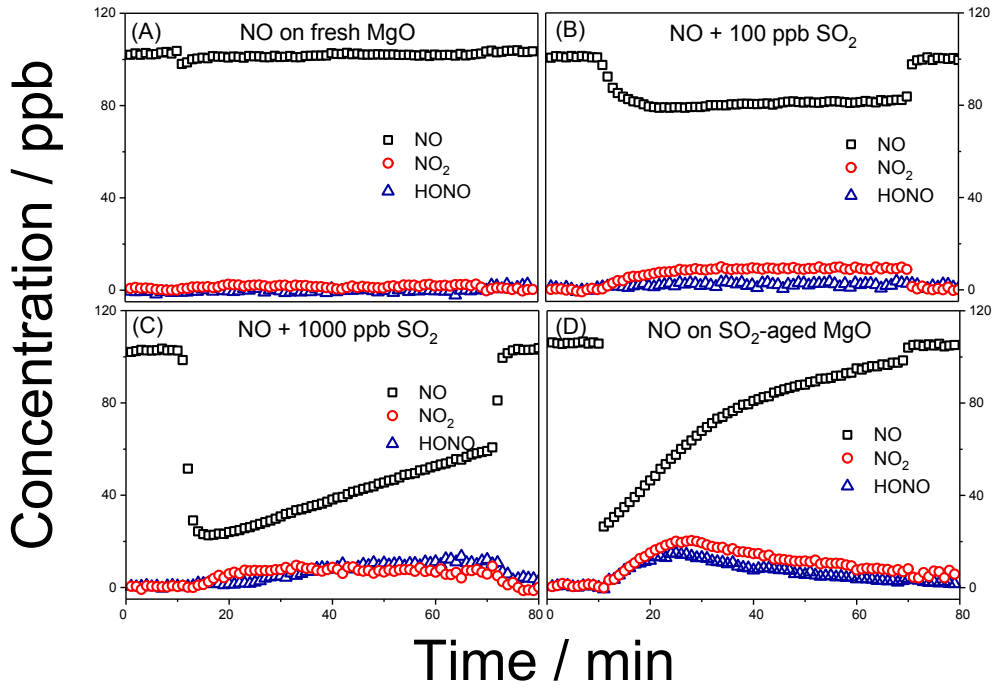

Figure 1. Concentrations of NO, NO_2 and HONO during flow tube experiments. (A) 100 ppb NO uptake on fresh MgO (41.66 mg); (B) 100 ppb NO uptake on fresh MgO (51.68 mg) with the coexistence of 100 ppb SO_2; (C) 100 ppb NO uptake on fresh MgO (29.39 mg) with the coexistence of 1000 ppb SO_2; (D) 100 ppb NO uptake on SO_2-aged MgO (30.14 mg). SO_2-aged MgO samples were online prepared during the experiments by exposing the tube which is covered with fresh MgO to 1000 ppb SO_2 for 4 h, then purged with synthetic air for 2 h to remove physically adsorbed surface species. Reaction conditions: RH=5%, T=295 K, total flow rate = 0.9 $L \cdot min^{-1}$.

The geometric uptake coefficient (γ_{geo}) of NO on fresh and SO_2-aged MgO as a function of sample masses are displayed in Figure 2. For fresh MgO, none NO uptake was observed and γ_{geo} are less than 1.0×10^{-6}, suggesting low reactivity of fresh MgO to NO. Unlike fresh samples, the γ_{geo} of NO increased significantly when NO coexisting with SO_2. When SO_2 concentration was up to 1000 ppb, the γ_{geo} of NO was quite similar to that on SO_2-aged MgO.

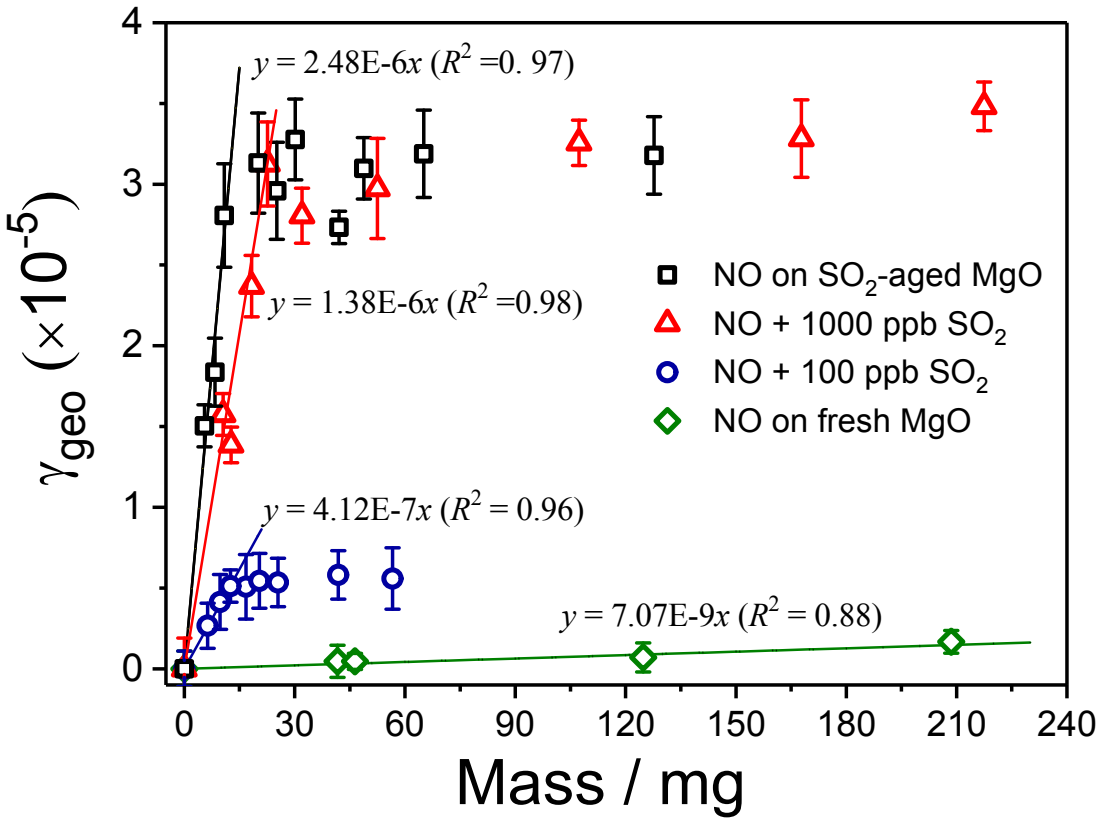

Figure 2. Mass dependence of initial geometric uptake coefficients (γ_{geo}) of 100 ppb NO on various MgO surfaces: SO_2-aged MgO (black), fresh MgO (olive), and fresh MgO coexisting with 1000 ppb SO_2 (red) and 100 ppb SO_2 (blue). RH=5%, T=295 K, total flow rate = 0.9 L·min^{-1}.

In an uptake experiment, the reactants will have a possibility to diffuse into the entire sample and the effective area may become equal to the S_{BET}. If the geometric uptake coefficients are proportional to the mass of the sample, then the effective surface area might approximate to the S_{BET}. As seen in Figure 2, linear relationship between γ_{geo} of NO and sample mass exists in all samples. Then, the true uptake coefficient (γ_{BET}) was obtained from the mass-dependence of γ_{geo} using Equation 3:[55, 56]

$$\gamma_{\mathrm{BET}} = \frac{S_{geo}}{S_{BET}} \times slope \qquad (3)$$

where S_{geo} is the geometric surface area (*i.e.* inner surface area of the sample tube, 69.08 cm^2), S_{BET} is 135.60 $cm^2 \cdot mg^{-1}$, and *slope* is the slope of the plot of γ_{geo} versus sample mass in the linear regime (mg^{-1}).

According to Equation 3, the γ_{BET} values of NO uptake were 3.60×10^{-9}, 2.10×10^{-7}, 7.03×10^{-7} and 1.26×10^{-6} on fresh MgO, on fresh MgO with coexisting 100 ppb or 1000 ppb SO_2, and on SO_2-aged MgO, respectively. SO_2 aging process leads to an increase of γ_{BET} by 2-3 orders of magnitudes, changing the inactive MgO to active surface for NO adsorption and reaction.

Surface species detection by *in situ* DRIFTS.

In situ DRIFTS experiments were conducted to further investigate the reaction mechanism of NO adsorption on SO_2-aged MgO particles. 200 ppb NO reaction on fresh MgO was firstly carried out and no surface species were observed after 4 h (as shown by the black line in Figure 3). This means no reaction of NO occurred on fresh MgO surface, which is in agreement with the results of flow tube experiments (Figure 1A).

For the reaction of NO on SO_2-aged MgO, MgO sample was first exposed to 1000 ppb SO_2 for 4 h and the surface was saturated with sulfur species (as illustrated by the red line in Figure 3). The peaks at 1265, 1190, 1160 and 1038 cm^{-1} could be assigned to sulfate/bisulfate species while the peak at 960 cm^{-1} was attributed to surface sulfite species on MgO.[41, 57] These results indicated that both sulfate and sulfite species were the surface products of SO_2 reaction on MgO, which is consistent with previous studies.[35, 57]

After purging with synthetic air for 2 h to remove the weakly adsorbed species, the SO_2-aged sample was further exposed to 200 ppb NO for 4 h (blue line in Figure 3). The peaks at 1265, 1190

and 1038 cm^{-1} due to sulfate increased significantly while the peak at 960 cm^{-1} due to sulfite decreased greatly, suggesting the conversion of sulfite to sulfate during the adsorption of NO. In a previous study, Ma et al.[41] found that a redox reaction between adsorbed sulfite and NO_2 could happen on MgO surface which led to the formation of nitrite/HONO and sulfate. Therefore, in the present study, we proposed that the gaseous product NO_2 from the heterogeneous oxidation of NO might be further converted to HONO coupling to the oxidation of surface sulfite to sulfate through a redox reaction.

It is interesting to note that the intensity of peak at 1160 cm^{-1} attributed to sulfate decreased. Meanwhile, two new peaks at 1714 and 1303 cm^{-1} were observed during the adsorption of NO. Previous study shown that when MgO particles were exposed to 200 ppm SO_2 and 200 ppm NO_2 simultaneously, two peaks at 1731 and 1298 cm^{-1} were observed and were assigned to surface N_2O_4.[35] However in the present study, it is not reasonable to assign these two peaks at 1714 and 1303 cm^{-1} to surface N_2O_4. Firstly, the low NO concentration used in this work (ppb level) limited the NO_2 generation and the consequent dimerization of NO_2 to N_2O_4. Secondly, these two peaks here were stable under continuous NO reaction and air purging, in contrast to Liu et al.[35] where N_2O_4 acted as an intermediate.

Previous studies about the interaction of NO_2 and SO_2 in solution proposed the initial step involves the formation of an addition complex [SO_3-NO_2].[24] This species could further undergo subsequent reaction with NO_2 to produce long lived intermediate [NO_2-SO_3-NO_2]. Two intermediates [SO_3NO_2] and [SO_3NO] were also proposed during the simultaneous adsorption of SO_2 and NO on Al_2O_3.[24] In this work, we assigned the peaks at 1714 and 1303 cm^{-1} to [SO_x-NO] complex species where SO_x might be SO_4 or SO_3. Because both sulfate and sulfite were detected

during the DRIFTS experiments, we further carried out DFT calculations to investigate the NO adsorption and reaction on fresh and SO_2-aged MgO surface.

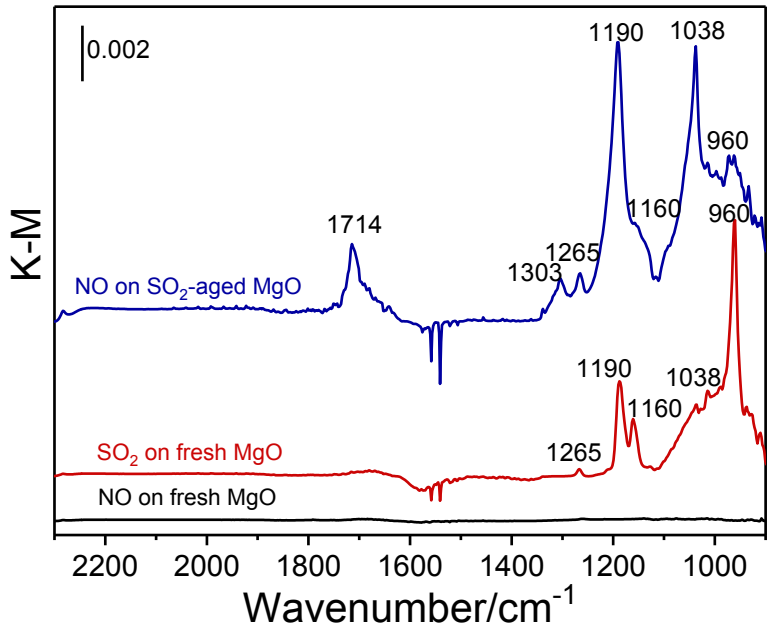

Figure 3. *In situ* DRIFTS spectra of 200 ppb NO reaction on SO_2-aged MgO (blue) and fresh MgO (black), and 200 ppb SO_2 reaction on fresh MgO (red). SO_2-aged MgO sample was prepared by exposing to 1000 ppb SO_2 for 4 h, and then purged with synthetic air for 2 h to remove weakly adsorbed species. Reaction conditions: T=295 K, RH=5%, total flow rate=200 mL·min^{-1}, reaction time=4 h.

DFT calculations of NO and SO_2 individual adsorption on fresh MgO(001) surface.

NO adsorption on fresh MgO was first investigated and three configurations for the NO adsorption on MgO(001) surface were taken into account. As shown in Figure 4A, the NO molecule adsorbs preferentially by the N atom on a surface O anion (η^1-N-top O) in a distance of 2.22 Å, with an adsorption energy (E_{ads}) of -0.20 eV. The calculated results are in good agreement with the findings in previous theoretical works.[58-60] The E_{ads} of N-down on bridge position (Figure 4B) appears to be approximate to the η^1-N-top O configuration, while N-down adsorption at Mg

cation (Figure 4C) is higher in E_{ads} compared to the most stable configuration (Figure 4A). The high adsorption energy and the long interaction distance indicated that the isolated NO weakly physisorbed on the fresh MgO(001) surface. In line with the flow tube and the DRIFTS experimental results, NO just undergoes reversible adsorption on the fresh MgO surface.

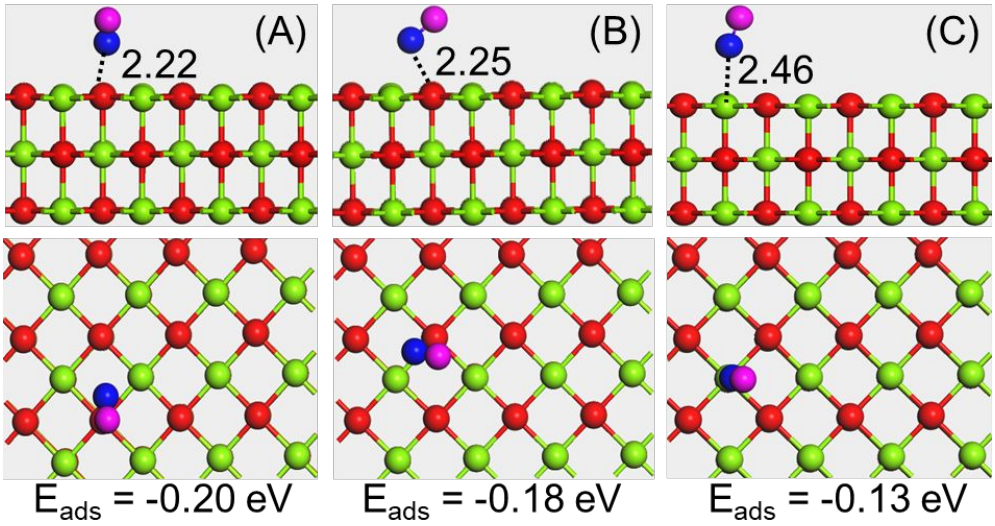

Figure 4. Side and top views of optimized structures of NO adsorption on the MgO(001) surface. (A) η^1-N-top O configuration; (B) N-down top bridge configuration; (C) η^1-N-top Mg configuration. Green, red, fuchsia, and blue balls represent Mg, lattice O, adsorbate O and N atoms, respectively. Only a part of the super cell has been visualized for a better overview. E_{ads}: adsorption energy.

The presence of surface adsorbed O_2 can oxidize NO to NO_2 via Elay-Rideal (Figure S2A) or Langmuir-Hinshelwood (Figure S2B) routes. However, the high adsorption energy of O_2 on MgO surface (-0.20 to 0.14 eV) restricted the occurrence of adsorbed O_2. Besides, the difficulty in NO adsorption, the high reaction energy barriers, as well as the low reaction heat also limited the probability of NO oxidation on fresh MgO.

As for sulfur species formed via SO_2 reaction on MgO(001) surface, *in situ* DRIFTS results showed that both sulfite and sulfate species were formed on MgO surface. DFT calculations identified that when SO_2 reacted on the MgO(001) surface, one sulfite configuration and four sulfate configurations were optimized. For the sulfite configuration (Figure S3A), the S atom of SO_2 adsorbs to the lattice O of the surface to form the SO_3-like sulfite. As for the sulfate species, the adsorption of SO_3 via S atom on a lattice O in the slab produced a SO_4-like sulfate (Figure S3B). Besides, three sulfate configurations formed via the binding of O atoms to surface Mg atoms were also built, including bidentate sulfate (Figure S3C), tridentate sulfate (Figure S3D) and quadridentate sulfate (Figure S3E). Compared to the bidentate and tridentate sulfates, the quadridentate sulfate exhibits severe deformation, and the energy of this configuration is much higher than those of other structures. Therefore, it is deduced that SO_3-like sulfite, SO_4-like, bidentate and tridentate sulfates are present on the MgO surface, and the adsorption and reaction of NO with these sulfur species were further conducted.

Mechanism of NO reaction on SO_2-aged MgO.

The configurations of NO adsorption to S or O atoms of SO_3-like sulfite are shown by Figure 5A and 5B, respectively. Compared to the NO adsorption on fresh MgO (Figure 4), both the adsorption energy as well as the interaction distance between NO and MgO surface increased due to the presence of SO_3-like sulfite. Besides, the long bond distance between NO and SO_3-like species (4.26 Å for N-S and 3.24 Å for N-O) indicated that there is no interaction between NO and SO_3-like species. All these results suggested that sulfite on the SO_2-aged MgO surface inhibited the NO adsorption. As for the MgO surface which covered by SO_4-like sulfate (Figure 5C), the

interaction distance between NO and MgO surface and the adsorption energy of NO were similar to those on fresh MgO, implying that SO_4-like sulfate has no influence on the NO adsorption.

In cases of MgO surface covered with bidentate (Figure 5D) and tridentate sulfates (Figure 5E), the N terminal of NO adsorbed to the O atom of sulfate. The NO adsorption energies varied from -2.19 to -1.95 eV, which are quite lower than the E_{ads} on fresh MgO, indicating that NO could chemisorb onto the surface via these sulfates. The vibration frequencies of N-O and S-O bands of these NO chemisorption products were calculated to be around 1750 cm^{-1} and 1270 cm^{-1} (Table S1). These vibrations were close to peaks detected in the DRIFTS experiments at 1714 cm^{-1} and 1302 cm^{-1} (Figure 3). Thus, it is considered that the promoted adsorption of NO could attribute to the presence of bidentate and tridentate sulfates, and [SO_4-NO] complex were the products for NO adsorption and reaction.

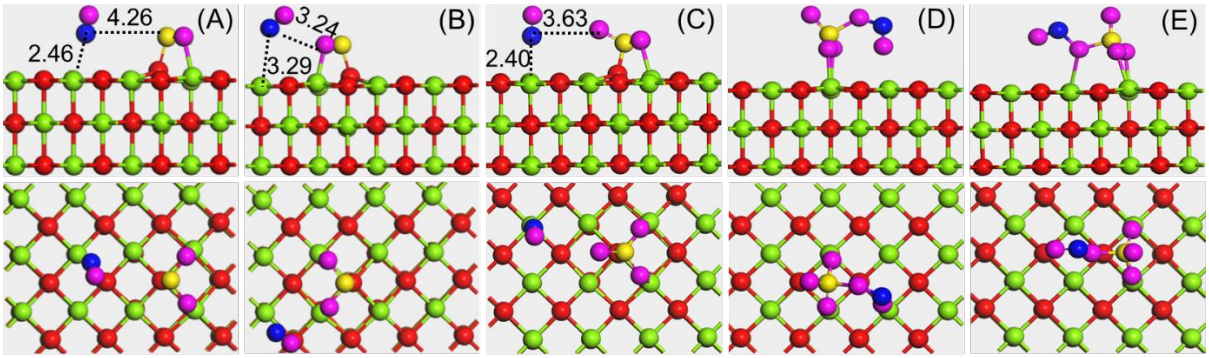

Figure 5. Possible adsorption configurations of NO on MgO surface with (A, B) SO_3-like sulfite, (C) SO_4-like sulfate, (D) bidentate sulfate, and (E) tridentate sulfate. Green, red, fuchsia, blue, and yellow balls represent Mg, lattice O, adsorbate O, N, and S atoms, respectively. Bond distance is in Å. E_{ads}: adsorption energy.

The fates of these [SO_4-NO] species were further calculated. As shown by the reaction pathway in Figure 6A, the complex [SO_4-NO] formed by NO adsorption on bidentate sulfate (as illustrated in Figure 5D) can be oxidized by O_2 to [O_3S-O-NO_2] species. Although this process is

303 exothermically (-1.05 eV), the high activation energy barrier (1.36 eV) makes the formation of
304 $[O_3S\text{-}O\text{-}NO_2]$ less likely.

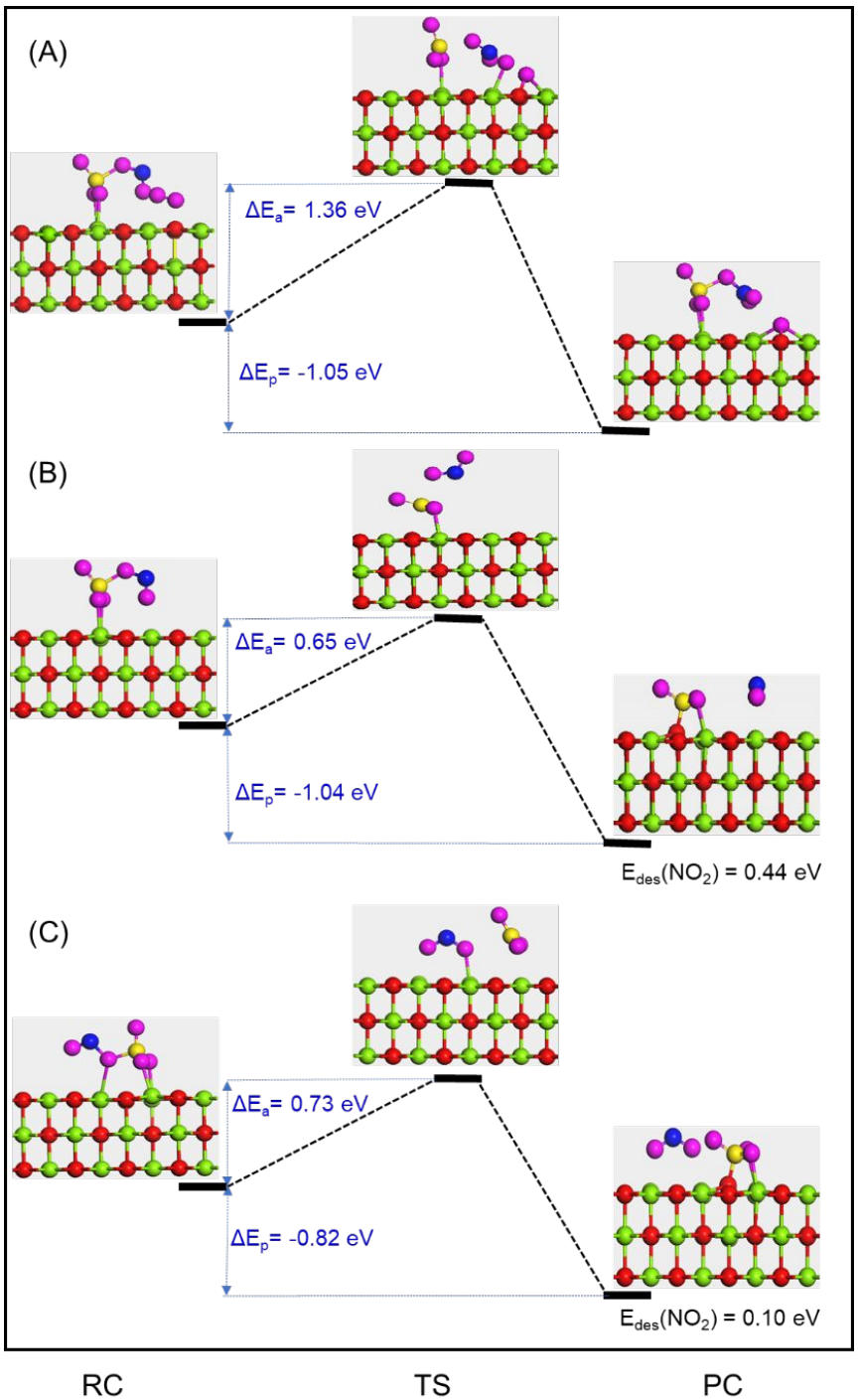

305
306 **Figure 6.** Reaction pathways of $[SO_4\text{-}NO]$ species. (A) Oxidation process of $[SO_4\text{-}NO]$ formed by NO
307 adsorption on bidentate sulfate; (B) Self-decomposition of $[SO_4\text{-}NO]$ formed by NO adsorption on bidentate

sulfate; (C) Self-decomposition of [SO_4-NO] formed by NO adsorption on tridentate sulfate. Optimized geometries for the reactant (RC), transition state (TS) and product (PC) are also presented. ΔE_a, ΔE_p and E_{des} refer to the reaction energy barrier, reaction heat, and the desorption energy of NO_2, respectively.

[SO_4-NO] formed by NO adsorption on bidentate sulfate could also undergo self-decomposition via the breakage of S-O bond and leads to the formation of SO_4-like species and gaseous NO_2 (Figure 6B). It should be noted that the energy barrier for self-decomposition (0.65 eV) is much lower than the oxidation process shown in Figure 6A. It can be concluded that the intermediate [SO_4-NO] self-decomposition is easily accessible since the lower energy barrier from the reactant to the product. Moreover, the heat released in this decomposition process (ΔE_p = -1.04 eV) benefits the desorption of NO_2 from the surface.

As for the reactant formed by NO adsorption with tridentate sulfate which is corresponding to [SO_4-NO] species in Figure 5F, the adsorbed NO can also abstract the O atom of adsorbed sulfate via the reaction pathway shown in Figure 6C. Similar to the reaction happened on bidentate sulfate, the NO adsorbed on tridentate sulfate can decompose to NO_2 and SO_4-like sulfate. Although the formed NO_2 can desorb from the surface spontaneously, the higher reaction energy barrier (0.73 eV) make this process is less possible compared to the reaction pathway in Figure 6B.

Combined the DFT calculation results and the DRIFTS experiments, we proposed a reaction mechanism for the promoted NO oxidation on SO_2-aged MgO. As shown by Scheme 1, NO adsorbs on bidentate and tridentate sulfates to form surface complex species [SO_4-NO]. Some [SO_4-NO] species are products of NO adsorption as illustrated by the peaks at 1714 and 1303 cm^{-1} in DRIFTS experiments (Figure 3), whereas other [SO_4-NO] complex act as intermediate and decompose to gaseous NO_2 and SO_4-like species. According to our previous work, the formed

NO_2 may further react with the surface sulfite to form nitrite, and the nitrite species could be adsorbed on MgO surface or released as gaseous HONO.[41]

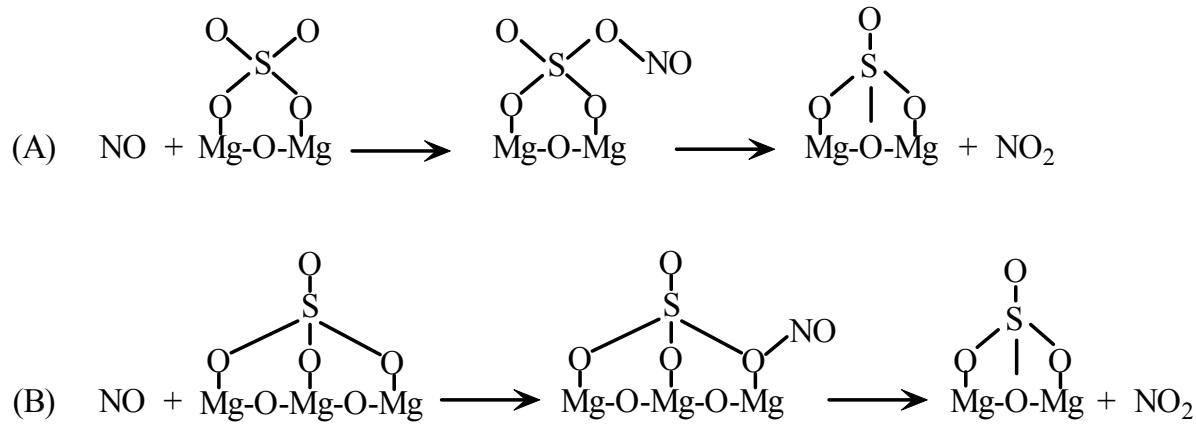

Scheme 1. Proposed mechanisms of NO adsorption and reaction on SO_2-aged MgO. (A) NO adsorbed on bidentate sulfate; (B) NO adsorbed on tridentate sulfate.

Atmospheric implications

In the past decades, heavy particulate pollution often occurs in winter in the northern China, in which the loading of secondary aerosol in $PM_{2.5}$ is very high.[61, 62] It has been recognized that these secondary components derived mainly from the oxidation of primary pollution due to anthropogenic emissions in the atmosphere.[61] However, for a long time, one of the puzzling problems is how the atmospheric oxidizing capacity emerged in winter since the solar radiation is weak, especially when the high concentration $PM_{2.5}$ dissipates light and limits the formation of O_3. The synergistic effect between NO and SO_2 found in the present study is helpful to dispel this puzzle. Mineral dust is a major aerosol composition. In China, it contributes ~35% of PM_{10} mass,[63] and accounts for 12-34% and 17-32% of winter and summer $PM_{2.5}$ mass, respectively.[64] Moreover, the dust from the Gobi desert significantly contributes to the heterogeneous conversion of primary components to secondary pollutions, and therefore is considered to be one of the important causes of haze in the North China Plain.[32, 65, 66] As demonstrated in this work, the true uptake coefficient

of NO on MgO with the presence of SO_2 was in the rage of 2.10×10^{-7}-1.26×10^{-6}, with the yields of NO_2 and HONO about 40% and 13-33%, respectively (Figure S4). According to the field measurement carried out in Beijing, the mean concentration of NO during a severe haze episode was 94 ppb with a maximum 214 ppb.[67] Thus, the mean formation rates of NO_2 and HONO via the heterogeneous reaction of NO and SO_2 on aerosol surface is estimated to be about 0.03-0.17 ppt·h^{-1} and 0.01-0.12 ppt·h^{-1}during the haze days (see detail in the Supporting Information). The promoted NO-NO_2 cycle and the enhanced HONO production will contribute to the atmospheric oxidizing capacity. It should be noted that recent studies demonstrated the critical role of the heterogeneous reactions in the formation of secondary particles during heavy haze.[32, 66, 68] Our study not only proved the importance of heterogeneous reaction on mineral oxides for the formation of secondary particles, but also revealed the role of these processes in enhancing the atmospheric oxidizing capacity independent of solar radiation through the activation of O_2 coupling with the conversion of NO to NO_2.

ASSOCIATED CONTENT

Supporting Information

The Supporting Information is available free of charge on the ACS Publications website at DOI:

Information as mentioned in the text. (PDF)

AUTHOR INFORMATION

Corresponding Author

* E-mail: qxma@rcees.ac.cn

ORCID

Chang Liu: 0000-0001-7497-8544

Qingxin Ma: 0000-0002-9668-7008

Jinzhu Ma: 0000-0003-1878-0669

Zhe Wang: 0000-0002-5627-6562

Tao Wang: 0000-0002-4765-9377

Author Contributions

§C. Liu and H. H. Wang contributed equally to this work.

Notes

The authors declare no competing financial interest.

ACKNOWLEDGMENT

This research was financially supported by the National Natural Science Foundation of China (21922610, 21876185, and 91744205). The authors also appreciate the Youth Innovation Promotion Association, CAS (2018055), and the Young Talent Project of the Center for Excellence in Regional Atmospheric Environment, CAS (CERAE201801).

REFERENCES

1. Crutzen, P. J., The role of NO and NO_2 in the chemistry of the troposphere and stratosphere. *Annu. Rev. Earth Planet. Sci.* **1979,** *7*, 443-472.

2. Logan, J. A., Nitrogen oxides in the troposphere: Global and regional budgets. *J. Geophys. Res.: Oceans* **1983,** *88*, (C15), 10785-10807.

3. Majewski, W. A.; Khair, M. K., *Diesel emissions and their control*. SAE International: 2006.

4. Grice, S.; Stedman, J.; Kent, A.; Hobson, M.; Norris, J.; Abbott, J.; Cooke, S., Recent trends and projections of primary NO_2 emissions in Europe. *Atmos. Environ.* **2009,** *43*, 2154-2167.

5. Wu, Y.; Zhang, S. J.; Li, M. L.; Ge, Y. S.; Shu, J. W.; Zhou, Y.; Xu, Y. Y.; Hu, J. N.; Liu, H.; Fu, L. X.; He, K. B.; Hao, J. M., The challenge to NOx emission control for heavy-duty diesel vehicles in China. *Atmos. Chem. Phys.* **2012,** *12*, 9365-9379.

6. Carslaw, D. C.; GlynRhys-Tyler, New insights from comprehensive on-road measurements of NOx, NO_2 and NH_3 from vehicle emission remote sensing in London, UK. *Atmos. Environ.* **2013,** *81*, 339-347.

7. Atkinson, R.; Baulch, D. L.; Cox, R. A.; Crowley, J. N.; Hampson, R. F.; Hynes, R. G.; Jenkin, M. E.; Rossi, M. J.; Troe, J., Evaluated kinetic and photochemical data for atmospheric chemistry: Volume I-gas phase reactions of Ox, HOx, NOx and SOx species. *Atmos. Chem. Phys.* **2004,** *4*, (6), 1461-1738.

8. Tsukahara, H.; Ishida, T.; Mayumi, M., Gas-phase oxidation of nitric oxide: Chemical kinetics and rate constant. *Nitric Oxide* **1999,** *3*, (3), 191-198.

9. Wei, L.; Zhou, J.; Wang, Z.; Cen, K., Kinetic modeling of homogeneous low-temperature multi-pollutant oxidation by ozone. *Ozone: Sci. Eng.* **2007,** *29*, (3), 207-214.

10. Tyndall, G. S.; Cox, R. A.; Granier, C.; Lesclaux, R.; Moortgat, G. K.; Pilling, M. J.; Ravishankara, A. R.; Wallington, T. J., Atmospheric chemistry of small organic peroxy radicals. *J. Geophys. Res.* **2001,** *106*, (D11), 12157-12182.

11. Lightfoot, P. D.; Cox, R.; Crowley, J.; Destriau, M.; Hayman, G.; Jenkin, M.; Moortgat, G.; Zabel, F., Organic peroxy radicals: kinetics, spectroscopy and tropospheric chemistry. *Atmos. Environ.* **1992,** *26*, (10), 1805-1961.

12. Gligorovski, S.; Strekowski, R.; Barbati, S.; Vione, D., Environmental implications of hydroxyl radicals (•OH). *Chem. Rev.* **2015,** *115*, (24), 13051-13092.

13. Monks, P. S., Gas-phase radical chemistry in the troposphere. *Chem. Soc. Rev.* **2005,** *34*, (5), 376-395.

14. Stone, D.; Whalley, L. K.; Heard, D. E., Tropospheric OH and HO_2 radicals: field measurements and model comparisons. *Chem. Soc. Rev.* **2012,** *41*, 6348-6404.

15. Enger, B. C.; Auvray, X.; Lødeng, R.; Menon, M.; Waller, D.; Rønning, M., Catalytic oxidation of NO to NO_2 for nitric acid production over a Pt/Al_2O_3 catalyst. *Appl. Catal., A* **2018,** *564*, 142-146.

16. Hong, Z.; Wang, Z.; Li, X., Catalytic oxidation of nitric oxide (NO) over different catalysts: an overview. *Catal. Sci. Technol.* **2017,** *7*, (16), 3440-3452.

17. Russell, A.; Epling, W. S., Diesel oxidation catalysts. *Catal. Rev.* **2011,** *53*, (4), 337-423.

18. Granger, P.; Parvulescu, V. I., Catalytic NOx abatement systems for mobile sources: from three-way to lean burn after-treatment technologies. *Chem. Rev.* **2011,** *111*, (5), 3155-3207.

19. Smeltz, A. D.; Delgass, W. N.; Ribeiro, F. H., Oxidation of NO with O_2 on Pt (111) and Pt (321) large single crystals. *Langmuir* **2010,** *26*, (21), 16578-16588.

20. Smeltz, A. D.; Getman, R. B.; Schneider, W. F.; Ribeiro, F. H., Coupled theoretical and experimental analysis of surface coverage effects in Pt-catalyzed NO and O_2 reaction to NO_2 on Pt (111). *Catal. Today* **2008,** *136*, (1-2), 84-92.

21. Ding, X.; Qiu, J.; Liang, Y.; Zhao, M.; Wang, J.; Chen, Y., New insights into excellent catalytic performance of the Ce-modified catalyst for NO oxidation. *Ind. Eng. Chem. Res.* **2019,** *58*, (19), 7876-7885.

22. Ishizuka, T.; Kabashima, H.; Yamaguchi, T.; Tanabe, K.; Hattori, H., Initial step of flue gas desulfurization an IR study of the reaction of SO_2 with NOx on CaO. *Environ. Sci. Technol.* **2000,** *34*, (13), 2799-2803.

23. Hadjiivanov, K.; Knözinger, H., Species formed after NO adsorption and NO + O_2 co-adsorption on TiO_2: an FTIR spectroscopic study. *Phys. Chem. Chem. Phys.* **2000,** *2*, (12), 2803-2806.

24. Xie, Y.; Chen, Y.; Ma, Y.; Jin, Z., Investigation of simultaneous adsorption of SO_2 and NO on γ-alumina at low temperature using DRIFTS. *J. Hazard. Mater.* **2011,** *195*, 223-229.

25. Cerruti, L.; Modone, E.; Guglielminotti, E.; Borello, E., Infra-red study of nitric oxide adsorption on magnesium oxide. *J Chem Soc, Faraday Trans* **1974,** *70*, 729-739.

26. Otto, K.; Shelef, M., The adsorption of nitric oxide on iron oxides. *J. Catal.* **1970,** *18*, (2), 184-192.

27. Saastad, O. W.; Ellermann, T.; Nielsen, C. J., On the adsorption of NO and NO_2 on cold H_2O/H_2SO_4 surfaces. *Geophys. Res. Lett.* **1993,** *20*, (12), 1191-1193.

28. Crowley, J. N.; Ammann, M.; Cox, R. A.; Hynes, R. G.; Jenkin, M. E.; Mellouki, A.; Rossi, M. J.; Troe, J.; Wallington, T. J., Evaluated kinetic and photochemical data for atmospheric chemistry: Volume V-heterogeneous reactions on solid substrates. *Atmos. Chem. Phys.* **2010,** *10*, 9059-9223.

29. Xue, J.; Yu, X.; Yuan, Z.; Griffith, S. M.; Lau, A. K. H.; Seinfeld, J. H.; Yu, J. Z., Efficient control of atmospheric sulfate production based on three formation regimes. *Nat. Geosci.* **2019,** *12*, (12), 977-982.

30. Xue, J.; Yuan, Z.; Griffith, S. M.; Yu, X.; Lau, A. K. H.; Yu, J. Z., Sulfate formation enhanced by a cocktail of high NOx, SO_2, particulate matter, and droplet pH during haze-fog events in megacities in China: an observation-based modeling investigation. *Environ. Sci. Technol.* **2016,** *50*, (14), 7325-7334.

31. Cheng, Y. Z., G.; Wei, C.; Mu, Q.; Zheng, B.; Wang, Z.; Gao, M.; Zhang, Q.; He, K.; Carmichael, G.; Pöschl, U.; Su, H., Reactive nitrogen chemistry in aerosol water as a source of sulfate during haze events in China. *Sci. Adv.* **2016,** *2*, e1601530.

32. He, H.; Wang, Y.; Ma, Q.; Ma, J.; Chu, B.; Ji, D.; Tang, G.; Liu, C.; Zhang, H.; Hao, J., Mineral dust and NOx promote the conversion of SO_2 to sulfate in heavy pollution days. *Sci. Rep.* **2014,** *4*, 4172.

33. Li, L.; Hoffmann, M. R.; Colussi, A. J., Role of nitrogen dioxide in the production of sulfate during Chinese haze-aerosol episodes. *Environ. Sci. Technol.* **2018,** *52*, (5), 2686-2693.

34. Wang, G.; Zhang, R.; Gomez, M. E.; Yang, L.; Zamora, M. L.; Hu, M.; Lin, Y.; Peng, J.; Guo, S.; Meng, J.; Li, J.; Cheng, C.; Hu, T.; Ren, Y.; Wang, Y.; Gao, J.; Cao, J.; An, Z.; Zhou, W.; Li, G.; Wang, J.; Tian, P.; Marrero-Ortiz, W.; Secrest, J.; Du, Z.; Zheng, J.; Shang, D.; Zeng, L.; Shao, M.; Wang, W.; Huang, Y.; Wang, Y.; Zhu, Y.; Li, Y.; Hu, J.; Pan, B.; Cai, L.; Cheng, Y.; Ji, Y.; Zhang, F.; Rosenfeld, D.; Liss, P. S.; Duce, R. A.; Kolb, C. E.; Molina, M. J., Persistent sulfate formation from London Fog to Chinese haze. *Proc. Natl. Acad. Sci. U. S. A.* **2016,** *113*, (48), 13630-13635.

35. Liu, C.; Ma, Q.; Liu, Y.; Ma, J.; He, H., Synergistic reaction between SO_2 and NO_2 on mineral oxides: a potential formation pathway of sulfate aerosol. *Phys. Chem. Chem. Phys.* **2012,** *14*, (5), 1668-1676.

36. Ma, Q.; Liu, Y.; He, H., Synergistic effect between NO_2 and SO_2 in their adsorption and reaction on γ-alumina. *J. Phys. Chem. A* **2008,** *112*, (29), 6630-6635.

37. Ullerstam, M.; Johnson, M. S.; Vogt, R.; Ljungstrom, E., DRIFTS and Knudsen cell study of the heterogeneous reactivity of SO_2 and NO_2 on mineral dust. *Atmos. Chem. Phys.* **2003,** *3*, (6), 2043-2051.

38. Liu, W.; He, X.; Pang, S.; Zhang, Y., Effect of relative humidity on O_3 and NO_2 oxidation of SO_2 on α-Al_2O_3 particles. *Atmos. Environ.* **2017,** *167*, 245-253.

39. Zhao, D.; Song, X.; Zhu, T.; Zhang, Z.; Liu, Y.; Shang, J., Multiphase oxidation of SO_2 by NO_2 on $CaCO_3$ particles. *Atmos. Chem. Phys.* **2018,** *18*, 2481-2493.

40. Yang, W.; Chen, M.; Xiao, W.; Guo, Y.; Ding, J.; Zhang, L.; He, H., Molecular insights into NO-promoted sulfate formation on model TiO_2 nanoparticles with different exposed facets. *Environ. Sci. Technol.* **2018,** *52*, (24), 14110-14118.

41. Ma, Q.; Wang, T.; Liu, C.; He, H.; Wang, Z.; Wang, W.; Liang, Y., SO_2 initiates the efficient conversion of NO_2 to HONO on MgO surface. *Environ. Sci. Technol.* **2017,** *51*, 3767-3775.

42. Monge, M. E.; D'Anna, B.; George, C., Nitrogen dioxide removal and nitrous acid formation on titanium oxide surfaces-an air quality remediation process? *Phys. Chem. Chem. Phys.* **2010,** *12*, (31), 8991-8998.

43. Underwood, G. M.; Miller, T. M.; Grassian, V. H., Transmission FT-IR and Knudsen cell study of the heterogeneous reactivity of gaseous nitrogen dioxide on mineral oxide particles. *J. Phys. Chem. A* **1999,** *103*, (31), 6184-6190.

44. Liu, Y.; Ma, Q.; He, H., Comparative study of the effect of water on the heterogeneous reactions of carbonyl sulfide on the surface of a-Al_2O_3 and MgO. *Atmos. Chem. Phys.* **2009,** *9*, 6273-6286.

45. Ma, J.; Liu, Y.; He, H., Heterogeneous reactions between NO_2 and anthracene adsorbed on SiO_2 and MgO. *Atmos. Environ.* **2010,** *45*, (4), 917-924.

46. Usher, C. R.; Michel, A. E.; Grassian, V. H., Reactions on mineral dust. *Chem. Rev* **2003,** *103*, (12), 4883-4940.

47. Tang, M.; Cziczo, D. J.; Grassian, V. H., Interactions of water with mineral dust aerosol: water adsorption, hygroscopicity, cloud condensation, and ice nucleation. *Chem. Rev.* **2016,** *116*, (7), 4205-4259.

48. Ndour, M.; Nicolas, M.; Danna, B.; Ka, O.; George, C., Photoreactivity of NO_2 on mineral dusts originating from different locations of the Sahara desert. *Phys. Chem. Chem. Phys.* **2009,** *11*, (9), 1312-1319.

49. Murphy, D. M.; Fahey, D. W., Mathematical treatment of the wall loss of a trace species in denuder and catalytic converter tubes. *Anal. Chem.* **1987,** *59*, (23), 2753-2759.

50. Cooney, D. O.; Kim, S.; Davis, E. J., Analyses of mass transfer in hemodialyzers for laminar blood flow and homogeneous dialysate. *Chem. Eng. Sci.* **1974,** *29*, (8), 1731-1738.

51. Kresse, G.; Furthmuller, J., Efficiency of ab-initio total energy calculations for metals and semiconductors using a plane-wave basis set. *Comp. Mater. Sci.* **1996,** *6*, (1), 15-50.

52. Blochl, P. E., Projector augmented-wave method. *Phys. Rev. B* **1994,** *50*, (24), 17953-17979.

53. Kresse, G.; Joubert, D., From ultrasoft pseudopotentials to the projector augmented-wave method. *Phys. Rev. B* **1999,** *59*, (3), 1758-1775.

54. Perdew, J. P.; Burke, K.; Ernzerhof, M., Generalized gradient approximation made simple. *Phys. Rev. Lett.* **1996,** *77*, (18), 3865-3868.

55. Underwood, G. M.; Li, P.; Usher, C. R.; Grassian, V. H., Determining accurate kinetic parameters of potentially important heterogeneous atmospheric reactions on solid particle surfaces with a Knudsen cell reactor. *J. Phys. Chem. A* **2000,** *104*, (4), 819-829.

56. Liu, Y.; Han, C.; Ma, J.; Bao, X.; He, H., Influence of relative humidity on heterogeneous kinetics of NO_2 on kaolin and hematite. *Phys. Chem. Chem. Phys.* **2015,** *17*, (29), 19424-19431.

57. Goodman, A. L.; Li, P.; Usher, C. R.; Grassian, V. H., Heterogeneous uptake of sulfur dioxide on aluminum and magnesium oxide particles. *J. Phys. Chem. A* **2001,** *105*, (25), 6109-6120.

58. Miletic, M.; Gland, J. L.; Hass, K. C.; Schneider, W. F., First-principles characterization of NOx adsorption on MgO. *J. Phys. Chem. B* **2003,** *107*, (1), 157-163.

59. Schneider, W. F.; Hass, K. C.; Miletic, M.; Gland, J. L., Dramatic cooperative effects in adsorption of NO_x on MgO(001). *J. Phys. Chem. B* **2002,** *106*, (30), 7405-7413.

60. Rodriguez, J. A.; Jirsak, J.; Kim, J. Y.; Larese, J. Z.; Maiti, A., Interaction of NO and NO_2 with MgO(100): photoemission and density-functional studies. *Chem. Phys. Lett.* **2000,** *330*, (3-4), 475-483.

61. Huang, R. J.; Zhang, Y.; Bozzetti, C.; Ho, K.-F.; Cao, J. J.; Han, Y.; Daellenbach, K. R.; Slowik, J. G.; Platt, S. M.; Canonaco, F.; Zotter, P.; Wolf, R.; Pieber, S. M.; Bruns, E. A.; Crippa, M.; Ciarelli, G.; Piazzalunga, A.; Schwikowski, M.; Abbaszade, G.; Schnelle-Kreis, J.; Zimmermann, R.; An, Z.; Szidat, S.; Baltensperger, U.; Haddad, I. E.; Prévôt, A. S. H., High secondary aerosol contribution to particulate pollution during haze events in China. *Nature* **2014,** *514*, 218-222.

520 62. Fu, H.; Chen, J., Formation, features and controlling strategies of severe haze-fog pollutions in China. *Sci.*
521 *Total Environ.* **2017,** *578*, 121-138.
522 63. Zhang, X. Y.; Wang, Y. Q.; Niu, T.; Zhang, X. C.; Gong, S. L.; Zhang, Y. M.; Sun, J. Y., Atmospheric
523 aerosol compositions in China: spatial/temporal variability, chemical signature, regional haze distribution and
524 comparisons with global aerosols. *Atmos. Chem. Phys.* **2012,** *12*, (2), 779-799.
525 64. Cao, J.; Shen, Z.; Chow, J. C.; Watson, J. G.; Lee, S.; Tie, X.; Ho, K.; Wang, G.; Han, Y., Winter and summer
526 $PM_{2.5}$ chemical compositions in fourteen Chinese cities. *J. Air Waste Manage. Assoc.* **2012,** *62*, (10), 1214-1226.
527 65. Wang, Y. S.; Yao, L.; L.Wang, L.; Liu, Z. R.; Ji, D. S.; Tang, G. Q.; Zhang, J. K.; Sun, Y.; Hu, B.; Xin, J.
528 Y., Mechanism for the formation of the January 2013 heavy haze pollution episode over central and eastern
529 China. *Sci China Earth Sci.* **2014,** *57*, (1), 14-25.
530 66. Zheng, B.; Zhang, Q.; Zhang, Y.; He, K. B.; Wang, K.; Zheng, G.; Duan, F.; Ma, Y.; Kimoto, T.,
531 Heterogeneous chemistry: a mechanism missing in current models to explain secondary inorganic aerosol
532 formation during the January 2013 haze episode in North China. *Atmos. Chem. Phys.* **2014,** *15*, (4), 2031-2049.
533 67. Zhang, W.; Tong, S.; Ge, M.; An, J.; Shi, Z.; Hou, S.; Xia, K.; Qu, Y.; Zhang, H.; Chu, B.; Sun, Y.; He, H.,
534 Variations and sources of nitrous acid (HONO) during a severe pollution episode in Beijing in winter 2016. *Sci.*
535 *Total Environ.* **2019,** *648*, 253-262.
536 68. Zheng, G. J.; Duan, F. K.; Su, H.; Ma, Y. L.; Cheng, Y.; Zheng, B.; Zhang, Q.; Huang, T.; Kimoto, T.;
537 Chang, D., Exploring the severe winter haze in Beijing: the impact of synoptic weather, regional transport and
538 heterogeneous reactions. *Atmos. Chem. Phys.* **2015,** *15*, (6), 2969-2983.

539